BIMETALLIC FeBiBTC MOFs AS AN EFFICIENT PHOTOCATALYST FOR RHODAMINE B DEGRADATION

VAN CUONG NGUYEN, TRINH BAO SON, PHAM HOANG AI LE*

Faculty of Chemical Engineering, Industrial University of Ho Chi Minh City, 12 Nguyen Van Bao, Ward Hanh Thong, Ho Chi Minh City 70000, Viet Nam.

**Corresponding author: phamhoangaile@iuh.edu.vn*

DOIs: https://www.doi.org/10.46242/jstiuh.v81i3.5983

Abstract. In this study, **bimetallic FeBiBTC MOFs** (FeBiBTC) were synthesised via the solvothermal method and used as a catalyst for the photodegradation of Rhodamine B (RhB) in aqueous solution. The structure of FeBiBTC was characterised using XRD, FT-IR, and SEM. The band gap of FeBiBTC was ~3.28 eV compared to ~3.68 eV of pristine BiBTC. FeBiBTC1 showed the best photocatalytic performance among the synthesized materials with a photodegradation efficiency of 99.58% for 120 min in the presence of H_2O_2. The photodegradation of RhB follows a pseudo-first-order model with a rate constant of 0.045 min^{-1}, which is much higher than that of BiBTC. The effects of catalyst dose, pH, dye concentration, and radical scavengers on the photodegradation efficiency were also investigated. The results indicated that the photogenerated electrons are the predominant reactive species. Additionally, the catalyst demonstrated good reusability with minimal activity loss and structural stability after 4 cycles.

Keywords. Bi-MOF, **bimetallic FeBiBTC MOFs**, Rhodamine B, photocatalysis, wastewater treatment, advanced oxidation processes.

1 INTRODUCTION

The rapid industrialization of the textile, pharmaceutical, and chemical industries has led to the discharge of large volumes of dyes in wastewater. This resulted in significant environmental and health consequences due to its high chemical stability, toxicity, and resistance to biodegradation. Rhodamine B (RhB) can induce allergic reactions and cause cutaneous and ocular discomfort. Inhalation induces coughing, throat irritation, dyspnea, and thoracic discomfort. Vomiting transpires throughout the digestive system and impacts the liver and kidneys. When amassed in significant quantities within the body, it induces numerous detrimental effects on the liver, kidneys, reproductive system, and brain system, potentially resulting in cancer. Dermal touch induces allergic responses. Inhalation may induce symptoms like chest constriction, dyspnea, throat pruritus, cough, and pharyngitis. Therefore, the development of a low-cost, green, and highly effective method for the removal of RhB is urgent and of interest to researchers. There are various methods for the removal of RhB, such as adsorption, biological method, filtration, coagulation, photocatalyst and advanced oxidation methods. Among these methods, the photocatalytic method was known to degrade the toxic textile dyes into small, nontoxic molecules in water [1].

Recently, metal-organic frameworks (MOFs) have been a class of materials that incorporate metal ions and organic linkers. MOFs have attracted attention as materials for environmental applications, especially as photocatalysts for the degradation of textile dyes, due to their high surface area, tunable porosity, and versatile structural design [2,3]. Among these, bismuth-based MOFs are of interest as photocatalysts for the degradation of organic dyes due to non-toxicity, biocompatibility, stability and unique electronic properties. However, the practical limitations of pristine Bi-MOFs are the synthesis method, low porosity, stability, and photocatalytic activity. Bimetallic metal–organic frameworks exhibit high photocatalytic efficiency due to their high porosity, stability, and recyclability [4–7]. Recent studies on BiBTC-based MOFs have demonstrated their potential for photocatalytic degradation of organic pollutants; however, their performance remains limited by rapid charge recombination and insufficient generation of reactive oxygen species. To overcome these limitations, the incorporation of transition metal species has been explored. In this work, a Fe-modified BiBTC material is developed. Fe species are introduced at low content and remain highly dispersed within the framework without forming distinct crystalline phases. More importantly, the system operates via a hybrid photocatalysis–photo-Fenton mechanism in which photogenerated electrons play a dominant role in activating both H_2O_2 and dissolved O_2, while the Fe^{3+}/Fe^{2+} cycle contributes secondarily to $^{\bullet}OH$ generation. This electron-driven pathway distinguishes the present

© 2026 Trường Đại học Công nghiệp thành phố Hồ Chí Minh

system from conventional photo-Fenton processes. It enables enhanced catalytic efficiency under mild conditions, providing new insight into the design of MOF-based catalysts with synergistic functionalities.

In this work, bimetallic FeBiBTC MOFs were prepared via a solvothermal method. The structural, optical, and photocatalytic properties were systematically investigated using FT-IR, XRD, SEM, UV–Vis DRS and XPS. The effects of various parameters on degradation efficiency, including dose, concentration, time, and pH, were studied. Moreover, the photocatalytic mechanism was investigated, providing insights into the efficiency of bimetallic MOF-based photocatalysts for wastewater treatment applications.

2 EXPERIMENTAL

2.1 Materials

$Bi(NO_3)_3 \cdot 5H_2O$ (≥98.0%), trimesic acid (H_3BTC, $C_9H_6O_6$, 95%), iron(III) nitrate, Rhodamine B, and 1,4-benzoquinone (≥99%) were sourced from Sigma-Aldrich. Sodium oxalate (≥99.8%), potassium dichromate (≥99.8%), N, N-dimethylformamide (DMF, 99%), and methanol (MeOH, CH_4O ≥99.5%) were acquired from Xilong Scientific Co., Ltd. All chemicals were analytical grade and used without further purification.

2.2 Synthesis of BiBTC and FeBi-MOF

BiBTC was synthesized via a solvothermal method. Briefly, $Bi(NO_3)_3 \cdot 5H_2O$ (0.15 g, 0.3 mmol) and H_3BTC (0.75 g, 3.5 mmol) were dissolved in a mixed solvent of DMF (30 mL) and methanol (30 mL) under magnetic stirring for 30 min to obtain a homogeneous solution. The mixture was then transferred into a Teflon-lined stainless-steel autoclave and heated at 120 °C for 24 h. After cooling to room temperature, the resulting precipitate was collected by centrifugation (6000 rpm, 10 min), washed three times with a DMF/MeOH (1:1, v/v) mixture and once with methanol, and subsequently dried at 80 °C for 24 h to obtain a pale yellow powder [8,9].

Bimetallic FeBiBTC (denoted as FeBiBTC1–3) were synthesized using the above procedure. Typically, $Fe(NO_3)_3 \cdot 9H_2O$ (0.0475 g) and $Bi(NO_3)_3 \cdot 5H_2O$ (0.085 g) were co-dissolved with H_3BTC (0.75 g) in a solvent mixture of methanol (30 mL) and DMF (30 mL). The solution was stirred for 30 min and subjected to solvothermal treatment at 120 °C for 24 h. The obtained products were isolated, washed, and dried to yield coloured powders.

2.3 Characterization

The crystal structure was analyzed by X-ray diffraction (XRD, LabX XRD-6100) and the functional groups were identified using FT-IR spectroscopy (Tensor 27 spectrometer, Bruker, Germany). Morphology was examined by SEM (FESEM, JEOL JSM-7401F, Tokyo, Japan). Optical properties were studied using UV–Vis and DRS spectroscopy (UV–Vis DRS, Cary 4000).

2.4 Photocatalytic degradation experiments

The photocatalytic performance of the as-prepared catalysts was evaluated via the degradation of Rhodamine B under visible-light irradiation. A 300 W Xe lamp equipped with a UV cut-off filter ($\lambda > 420$ nm) was employed as the light source to simulate visible light. In a typical experiment, 10 mg of catalyst was dispersed in 50 mL of RhB aqueous solution with a desired initial concentration (typically 50 ppm). Before irradiation, the suspension was magnetically stirred in the dark for 30 min to establish adsorption–desorption equilibrium between the catalyst surface and dye molecules. Subsequently, a specific amount of H_2O_2 (typically 0.1 mL) was added to the reaction system, and the mixture was irradiated with visible light under continuous stirring. At predetermined time intervals, approximately 3 mL of the suspension was withdrawn, centrifuged at 6000 rpm for 5 min to remove solid particles. The concentration of RhB was determined by measuring a UV–Vis spectrophotometer at 554 nm. The degradation efficiency of RhB was calculated using Equation (1). The reaction kinetics were analyzed using a pseudo-first-order kinetic model (Equation 2):

$$H(\%) = \frac{C_0 - C_t}{C_0} \times 100 \qquad (1)$$

$$\ln\left(\frac{C_0}{C_t}\right) = kt \qquad (2)$$

where C_0 and C_tt is the initial RhB concentration and the RhB concentration at reaction time t, respectively, and k(min^{-1}) is the rate constant.

The effects of various parameters on the photodegradation efficiency were studied by varying the catalyst dosage from 5 to 20 mg, the initial RhB concentration from 10 to 70 ppm, the H_2O_2 dosage to 0.1 mL, and the solution pH from 2 to 10. The pH of the solution was adjusted with HCl or NaOH. Radical-trapping experiments were conducted to identify the dominant reactive species by introducing specific scavengers into the reaction solution. The benzoquinone (BQ) for superoxide radicals ($^{\bullet}O_2^-$), isopropanol (IPA) for hydroxyl radicals ($^{\bullet}OH$), and ammonium oxalate (AO) for photogenerated holes (h^+) was added. The catalyst's reusability was tested over four consecutive cycles. After each run, the catalyst was collected by centrifugation, washed with deionized water and ethanol, dried at 80 °C, and reused. Control experiments in the absence of catalyst, light, or H_2O_2 were also conducted.

3 RESULTS AND DISCUSSION

3.1 Characterization

The FT-IR spectra of BiBTC and FeBiBTC samples (1–3) are shown in Figure 1a. The results confirmed the successful incorporation of Fe without disrupting the MOF framework. BiBTC and FeBiBTC showed a broad band at about 3400 cm^{-1}, which was attributed to O–H stretching. The peaks at 1600-1550 cm^{-1} and 1450-1400 cm^{-1} were attributed to the asymmetric and symmetric stretching vibrations of carboxylate groups (–COO$^-$), respectively. The FT-IR spectrum of FeBiBTC showed slight shifts in these bands upon Fe addition. The intensity of these peaks decreased with increasing Fe content in the FeBiBTC. At the low wavenumber region, the BiBTC showed a Bi–O band at 550-520 cm^{-1}, while Fe-modified samples decreased the intensity of Bi–O band and presented an additional band at 480-500 cm^{-1} assigned to Fe–O stretching. The intensity peaks were increased with increasing FeBiBTC from 1 to 3. The absence of a band at 1700 cm^{-1} (C=O of the –COOH group) showed that the ligands were completely coordinated. Finally, these results reveal that the bimetallic Fe–Bi framework was successfully prepared, with strong electronic interaction between the metal centres (Figure 1a).

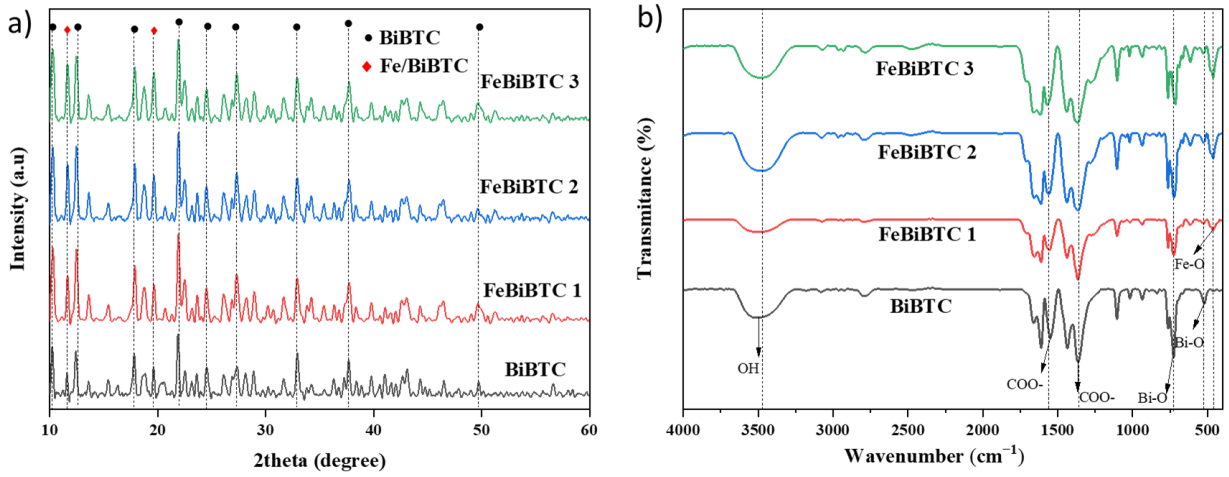


Figure 1: (a) FT-IR spectra and (b) XRD patterns of prepared samples.

The BiBTC and FeBiBTC XRD patterns are presented in Figure 1b. The results prove that the crystalline MOF structure remained unchanged after Fe addition. Pristine BiBTC shows characteristic diffraction peaks at 2θ ≈ 10.8°, 12.5°, 17.8°, 19.6°, 21.5°, 24.3°, 26.7°, 28.5°, 32.8°, 36.9°, and 49.8°, indicative of a well-defined framework. These peaks are also observed in all FeBiBTC samples, with no significant shifts in position. The results indicated that the crystal structure remains intact. It is important to note that there are no additional peaks corresponding to Fe_2O_3 or Fe_3O_4 in the XRD. This suggests that Fe species are highly dispersed or incorporated into the framework rather than forming separate crystalline phases. The

intensity of these peaks decreases, and a minor broadening occurs as the Fe content increases relative to pristine BiBTC. The intensities of the 10.8° and 19.6° peaks increased with increasing Fe content in FeBiBTC. This suggests that the crystals are less crystalline and that their lattices are distorted because some of the Bi^{3+} ions are replaced by smaller Fe^{3+} ions. These structural changes suggest that disorders are forming, thereby strengthening charge separation and photocatalytic activity [10,11].

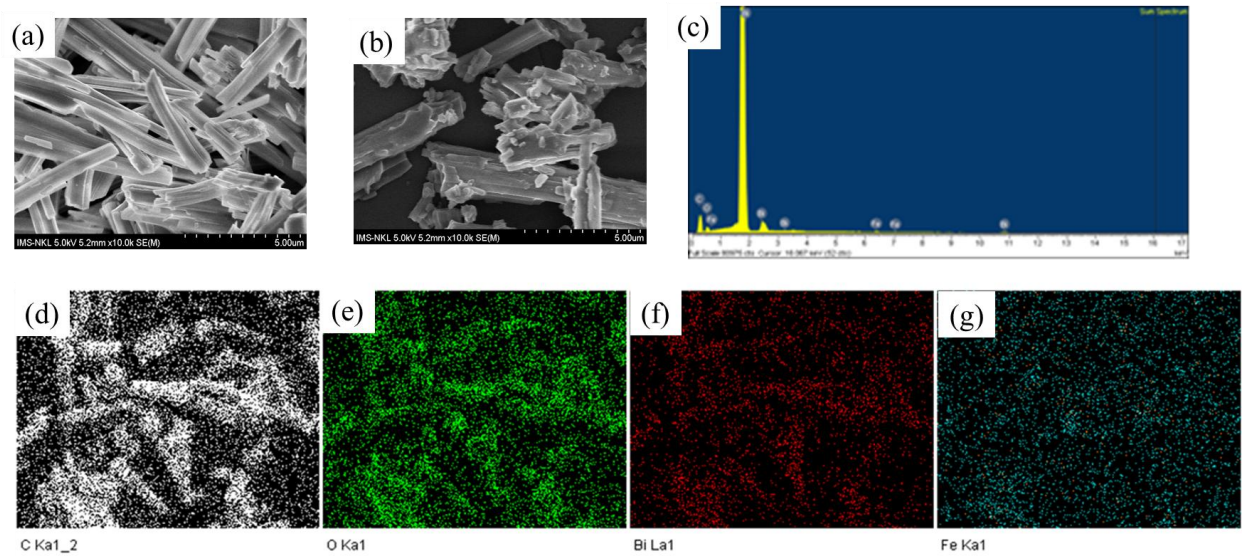


Figure 2: SEM images of (a) BiBTC, (b) FeBiBTC1; (c) EDS spectra FeBiBTC1, (d)-(g) EDX mapping FeBiBTC1

The SEM images of pristine BiBTC show uniform, rod-like structures with smooth surfaces and diameters of 200-450 nm, indicating well-controlled anisotropic crystal growth. The rod morphology remains unchanged after Fe incorporation. The surface is rougher than BiBTC. A similar result has been reported previously [12]. The EDX analysis confirms the presence of Fe (1.08 wt%, 0.32 at%) in the material, indicating successful incorporation of Fe into the BiBTC framework. In addition, elemental mapping shows a homogeneous distribution of Fe without detectable aggregation. The low Fe content and high dispersion explain the absence of distinct Fe-related peaks in the XRD patterns. Therefore, the combined XRD and EDX results consistently support the formation of a bimetallic FeBi-MOF rather than segregated iron oxide phases.

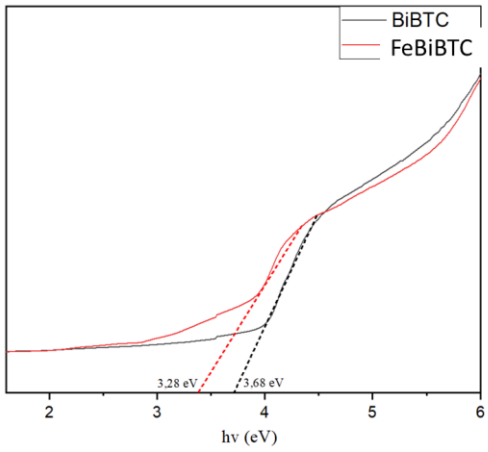


Figure 3: UV–Vis diffuse reflectance spectra (UV–Vis DRS) of FeBiBTC1.

Figure 3 shows the UV–Vis DRS spectra of BiBTC and FeBiBTC with different Fe contents. The results indicated that Fe incorporation significantly enhances the optical properties of BiBTC. The band gap decreases from 3.68 eV to 3.28 eV for BiBTC and FeBiBTC1, respectively. This can be explained by a clear red shift toward the visible region, and it may improve light harvesting. The decrease in band gap is

attributed to Fe-induced electronic states. This observation is consistent with the XPS results. The existence of these states enhances ligand- to -metal charge transfer and promotes electron excitation under visible light. The enhanced absorption and extended absorption tail suggest improved charge-carrier generation. The result is consistent with the dominant role of photogenerated electrons in radical trapping experiments. Therefore, the Fe modification in FeBiBTC led to efficient electron-transfer pathways, thereby enhancing the photocatalytic performance of FeBiBTC1 under visible-light irradiation.

The XPS result was presented in Figure 4. XPS results confirm the surface elemental composition and chemical valence states of the FeBiBTC. The elemental composition of the FeBi-MOF was further analyzed by EDX. The spectrum (Figure 4a) confirms the coexistence of Fe, Bi, C, and O in the FeBiBTC. The results showed the successful incorporation of both metal centres and organic ligands, with no detectable impurities. The Fe 2p spectrum presents the broad and relatively low intensity peaks at 711.2 eV and 724.5 eV for Fe $2p_{3/2}$ and (Fe $2p_{1/2}$, respectively (Figure 4b). It indicated the characteristic of the Fe^{3+} species coordinated with oxygen. This result was consistent with Fe^{3+} binding energies in Fe-based photocatalysts previously [12]. The Bi 4f spectrum displays two resolved peaks at 158.5 eV and 163.8 eV for Bi $4f_{7/2}$ and Bi $4f_{5/2}$, respectively. This confirmed the presence of Bi^{3+} in a coordinated state. A similar study was reported for values for the Bi^{3+} species [13]. The C 1s spectrum can be deconvoluted into components at 284.8 eV and 288.5 eV, which are attributed to aromatic C–C/C=C bonds and O–C=O groups of the BTC ligand, respectively (Figure 4d). Additionally, Figure 4e shows the O 1s spectrum, with a peak at 531.4 eV corresponding to coordinated carboxylate groups ($–COO^-$). The XPS analysis finally confirms that Fe is present as Fe^{3+} and Bi as Bi^{3+} in the FeBiBTC.

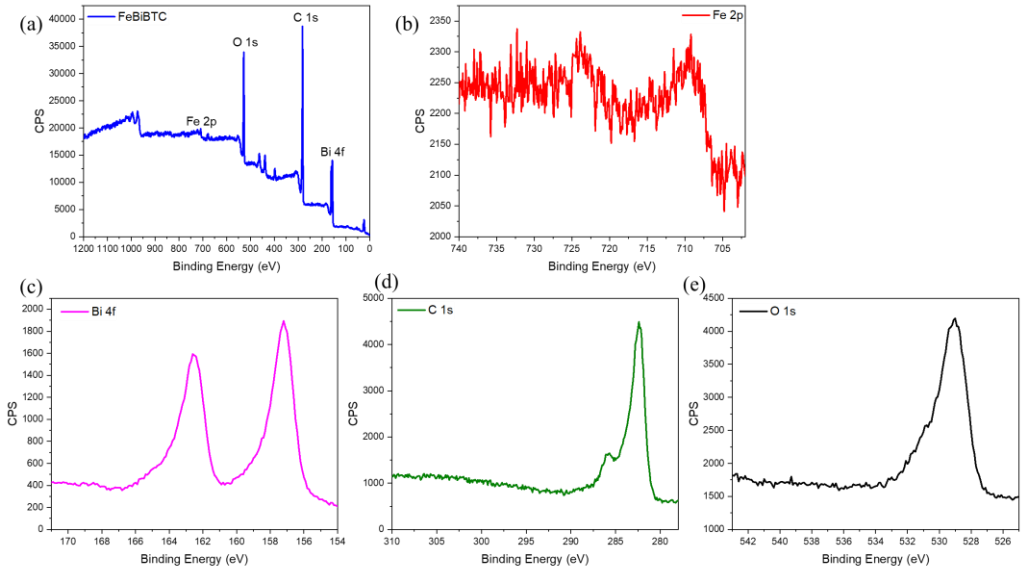


Figure 4: (a) XPS survey spectrum, (b) Fe 2p, (c) Bi 4f, (d) C 1s, and (e) O 1s spectra of FeBiBTC.

3.2 Photocatalytic degradation of RhB

The photodegradation results show that only the FeBiBTC catalyst achieves approximately 65–70% for RhB degradation after 120 min. However, FeBiBTC in the presence of H_2O_2 results in rapid photodegradation of RhB with 85% degradation efficiency within the first 30 min and reach 99% after 120 min. This result clearly indicates an enhancement of H_2O_2 in photocatalysis. Additionally, the RhB concentration remains nearly constant (100%) for up to 120 min under visible light in the absence of a catalyst. Throughout the photolysis reaction is insignificant. Similarly, the RhB with the presence of H_2O_2 exhibits minimal photodegradation, which indicates that direct oxidation by H_2O_2 is ineffective under visible light conditions (Figure 5a).

The effect of irradiation time on removal efficiency was also investigated at concentrations of 40-70 ppm and irradiation times of 15-120 min. The photodegradation efficiencies of both BiBTC and FeBIBTC

increased with increasing irradiation time. After 15 min of irradiation, BiBTC achieves only 57.65% RhB removal, whereas FeBiBTC1 shows a higher efficiency of 74.59%. In contrast, the low efficiencies were 12.99 and 21.61% for FeBiBTC2 and FeBiBTC3, respectively. However, the degradation efficiencies were 95.98, 99.58, 97.36, and 98.15% for BiBTC, FeBiBTC1, FeBiBTC2, and FeBiBTC3, respectively, after 120 min of irradiation. These results confirm that Fe incorporation enhances photocatalytic performance with a higher reaction rate than that of BiBTC. The efficacy of FeBiBTC1 indicates that the iron in the MOFs enhances the charge separation and reactive oxygen species formation. The diminished activity of FeBiBTC2 and FeBiBTC3 may result from an overabundance of iron species functioning as recombination centres or partially obstructing active sites (Figure 5b).

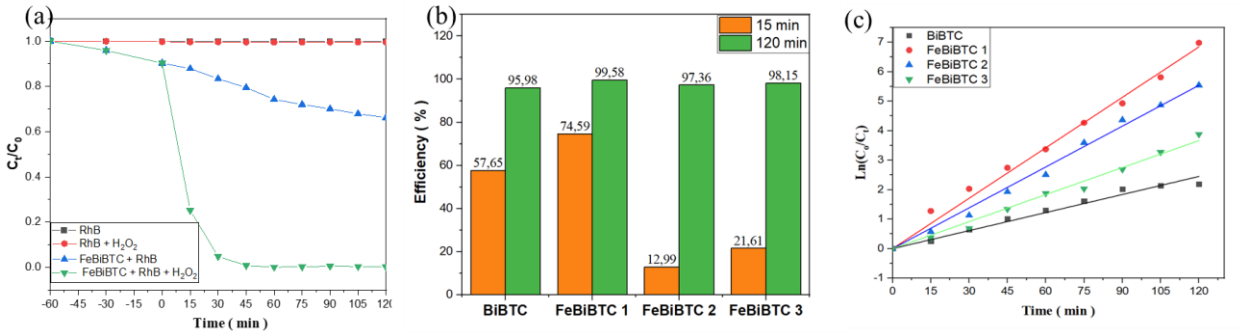


Figure 5: (a) Photocatalytic degradation of RhB under visible-light irradiation, (b) the effect of various materials, and (c) Pseudo-first-order kinetic plots

The kinetic study of RhB photodegradation follows pseudo-first-order kinetics with a strong linear relationship between $\ln(C_0/C_t)$ and reaction time. The correlation coefficients are all greater than 0.99. Adding Fe to the MOFs increases the rate constant relative to pristine BiBTC. An increase in Fe concentration in FeBiBTC decreases the rate constant. The rate constants were 0.012 min^{-1}, 0.02 min^{-1} and 0.025 min^{-1} for BiBTC, FeBiBTC3 and FeBiBTC2, respectively. The highest rate constant was observed for FeBiBTC1 (0.045 min^{-1}), which is more than three times that of BiBTC. These findings are consistent with the degradation efficiencies and confirm that the reaction kinetics are substantially enhanced by Fe incorporation (Figure 5c).

3.3 Effect of various factors

The catalyst dosage significantly affects the photocatalytic efficacy of FeBiBTC1 (Figure 6a). A similar RhB adsorption capacity (10-15%) was observed after 60 min for all samples. Increasing the catalyst dose from 0.005 to 0.015 g markedly improves degradation efficiency. As a result, the photocatalytic efficiencies were 94.6, 99.18, 99.10, and 95.97% for catalyst dosages of 0.005, 0.01, 0.015, and 0.02 g, respectively. Photodegradation was nearly complete at dosages of 0.015 and 0.02 g after 90 min. Further raising the catalyst loading above 0.02 g results in a decrease in efficiency to 95.97%. A higher catalyst loading provides more active sites for photocatalytic reactions, thereby increasing photodegradation efficiency. However, excessive catalyst loading may hinder light penetration due to increased turbidity or promote particle aggregation, thereby reducing the effective active surface area.

The effect of different initial RhB concentrations on the photocatalytic performance of FeBiBTC1 was evaluated over the range of 40-70 ppm. The results show that concentration significantly affects RhB degradation efficiency. Increasing the concentration decreases the degradation efficiency. The efficiencies are 94.08, 94.90, 91.49, and 82.20% for RhB concentrations of 40, 50, 60, and 70 ppm, respectively. The highest photodegradation efficiencies are detected with concentrations of 40 and 50 ppm. The RhB molecules in solution increased as the RhB concentration increased, while the number of active sites on the FeBiBTC surface remained constant with the same catalyst amount. This results in saturation at the catalytically active site, leading to diminished RhB photodegradation. Moreover, high RhB concentrations may inhibit light penetration into the solution and hinder contact between the catalyst and the solution, thereby decreasing degradation efficiency.

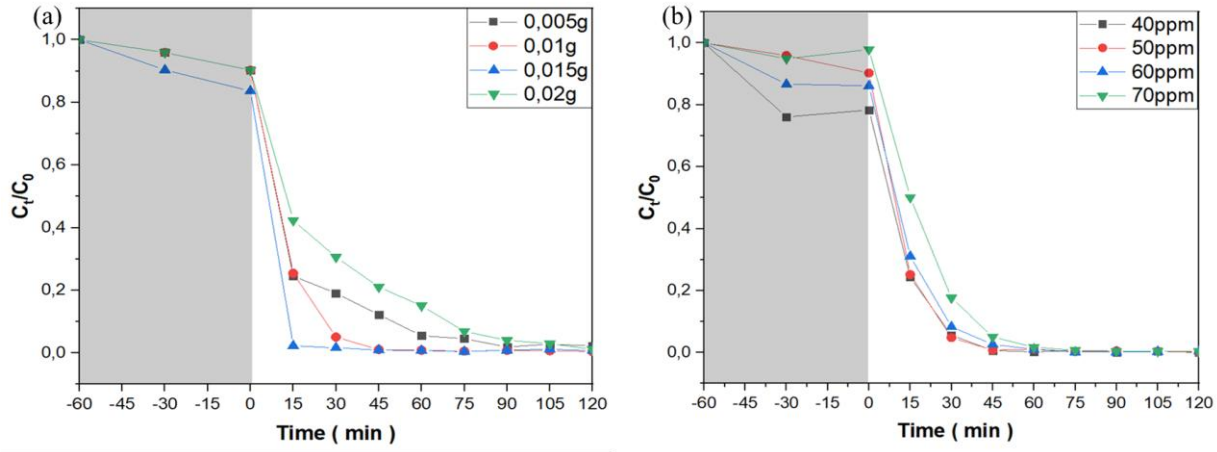


Figure 6: Effects of (a) catalyst dosage and (b) initial RhB concentration on the photodegradation efficiencies of FeBiBTC1

The solution pH plays a critical role in regulating the photocatalytic degradation of RhB over FeBiBTC1. The photodegradation of RhB decreased with increasing solution pH. In detail, the photocatalytic efficiencies at pH 3, 4, 5, 6, 7, and 9 are 60.51, 74.59, 62.47, 60.52, 17.72, and 20.02%, respectively, at 15 min. Moreover, the efficiencies are 97.1, 99.58, 98.67, 98.67, 81.47, and 80.73% for pH 3, 4, 5, 6, 7, and 9, respectively, after 120 min. The high performance in acidic media can be explained by the catalyst's point of zero charge ($pH_pzc = 3.4$). At pH values above 3.4, the catalyst surface becomes negatively charged, while at pH < 3.4, it is positively charged. Since RhB is predominantly present as a cationic dye in aqueous solution. At pH values above pH_pzc (4-6), the catalyst surface is negatively charged, enhancing electrostatic attraction between FeBiBTC and RhB molecules. The interaction promotes adsorption and facilitates subsequent photocatalytic oxidation. In contrast, under strongly alkaline conditions (pH 7–9), the degradation efficiency decreases significantly due to the reduced electrostatic attraction between FeBiBTC and RhB molecules (Figure 7a). A similar result was reported elsewhere [13].

Radical scavenging experiments were performed to identify the dominant reactive species involved in the photocatalytic degradation of RhB on FeBiBTC1. Various scavengers with a concentration of 100 µM were introduced into the reaction system, including EDTA as a hole (h^+) scavenger, $K_2Cr_2O_7$ as an electron (e^-) scavenger, ethanol (EtOH) as a hydroxyl radical ($^{\bullet}OH$) scavenger, and benzoquinone (BQ) as a superoxide radical ($^{\bullet}O_2^-$) scavenger. In the absence of scavengers, nearly complete photodegradation was observed within 60 min. However, when 100 µM $K_2Cr_2O_7$ was added, the photocatalytic efficiency decreased significantly compared to the other scavenger-containing systems. In contrast, the addition of EDTA, EtOH, or BQ caused only moderate inhibition of the degradation process. The suppression observed with $K_2Cr_2O_7$ indicates that photogenerated electrons play a crucial role in the degradation mechanism. It can explain that RhB degradation is predominantly driven by photogenerated electrons and electron-derived reactive species (via electron-mediated oxygen activation pathways). Meanwhile, h^+, $^{\bullet}OH$ and $^{\bullet}O_2^-$ radicals are not the primary contributors to the photodegradation of RhB. These results confirm that the electron transfer pathway is the dominant mechanism governing RhB photodegradation on FeBiBTC 1 (Figure 7b).

The role of H_2O_2 in this system is clarified as the process is not a purely photocatalytic reaction but rather a hybrid photocatalysis–photo-Fenton mechanism. Photogenerated electrons play a dominant role, as evidenced by the strong inhibition observed in the presence of $K_2Cr_2O_7$. These electrons can activate both H_2O_2 and dissolved O_2, generating reactive oxygen species. In this result, H_2O_2 acts not only as an oxidant but also as an electron acceptor, facilitating $^{\bullet}OH$ formation. Meanwhile, Fe species in the FeBiBTC participate in a Fe^{3+}/Fe^{2+} redox cycle, therefore contributing to $^{\bullet}OH$ generation via Fenton-like reactions. However, this contribution is secondary compared to the electron-driven pathway. Light irradiation further promotes the regeneration of Fe^{2+} from Fe^{3+} in the catalytic cycle. Therefore, the system can be described

as a photocatalytic process assisted by Fenton reactions, in which the electron-transfer pathway predominates over a conventional photo-Fenton process (Figure 8).

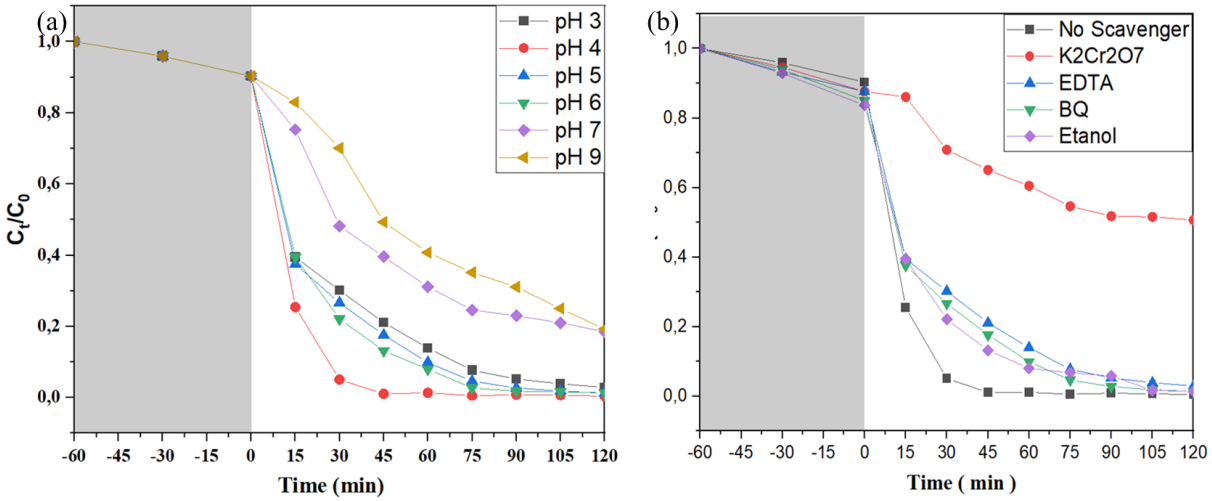


Figure 7: Effects of (a) pH on the photodegradation efficiencies and (b) Radical trapping experiments for RhB degradation of FeBiBTC1.

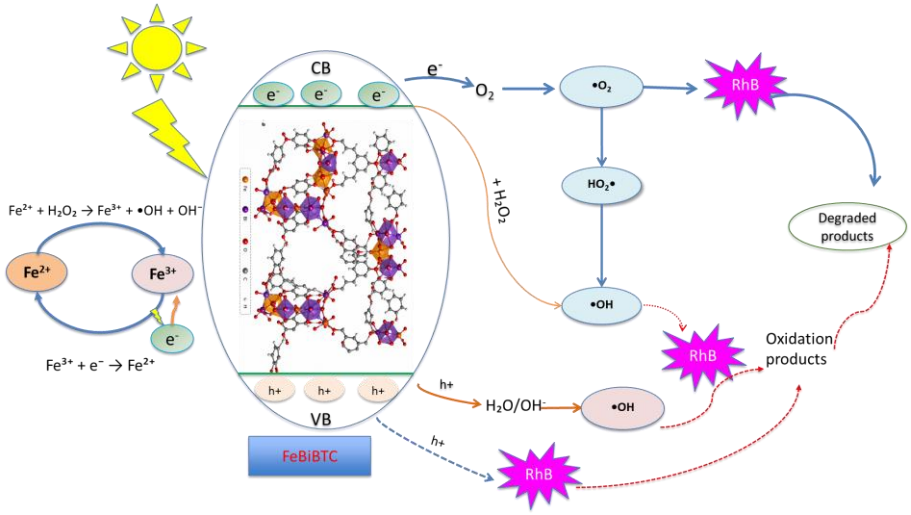


Figure 8: Proposed pathway for RhB degradation of FeBiBTC1.

The recyclability of FeBiBTC was evaluated over four consecutive photocatalytic cycles for RhB degradation under visible light irradiation (Figure 9a). The photodegradation efficiencies for the 1st, 2nd, 3rd, and 4th cycles are 98.64, 98.37, 99.41, and 99.32%, respectively. The result demonstrates that the catalytic performance remains nearly unchanged after several uses. To further assess structural stability, XRD patterns of the fresh catalyst and the recovered sample after four cycles were compared (Figure 9b). The diffraction peaks of the used catalyst matched those of the pristine FeBiBTC1, with no observable peak shifts, disappearances, or new diffraction signals. The maintenance of characteristic reflections indicates that the crystalline framework remains undamaged during repeated photocatalytic reactions.

The FT-IR spectra of FeBiBTC1 before and after photocatalytic reaction (Figure 9c) also confirm the chemical stability of the material. The vibrational bands associated with coordinated carboxylate groups (C=O stretching), aromatic C=C bonds, and metal–oxygen (Fe-O/Bi-O) interactions remain essentially unchanged after four cycles. No new absorption bands or significant shifts are observed, indicating that the coordination environment and organic linker structure are preserved.

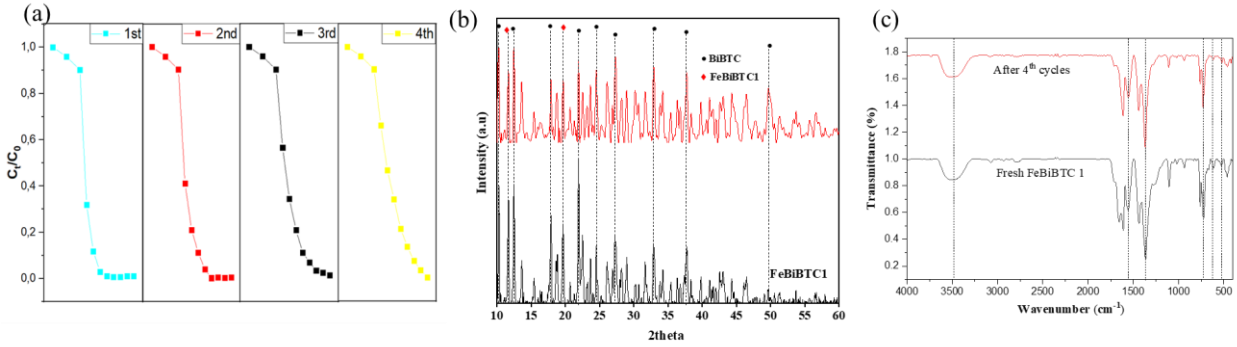


Figure 9: (a) Recycling performance of FeBiBTC1 for the photocatalytic degradation of RhB under visible-light irradiation, (b) XRD patterns of the catalyst before and after the photocatalytic reaction and (c) FT-IR spectra of the catalyst before and after use.

4 CONCLUSIONS

FeBiBTC was successfully synthesized via a solvothermal method. The structures were characterized by XRD, FT-IR, and SEM. The result indicated that Fe effectively modified the electronic structure without disrupting the MOF framework. FeBiBTC1 demonstrated the highest RhB photodegradation efficiency of 99.58% RhB degradation within 120 min and a significantly higher reaction rate. Additionally, the photodegradation efficiency was strongly affected by the initial RhB concentration. The efficiency was 82.20% at 70 ppm and increased to 99.58% at 40 ppm. Similarly, photodegradation efficiencies were 99.58% at pH 4 and 80.73% at pH 9. This enhancement is mainly attributed to improved charge separation and electron-mediated pathways, where photogenerated electrons and $^{\bullet}O_2^-$ are the dominant reactive species. In addition, the catalyst exhibited excellent stability and reusability across multiple cycles, with no noticeable structural changes. These results demonstrate that Fe incorporation is an effective strategy for enhancing Bi-MOF photocatalysts and offering promising potential for wastewater treatment applications.

ACKNOWLEDGMENT

The authors would like to thank the Industrial University of Ho Chi Minh City for financial support under grant number 105/HD-DHCN.

REFERENCES

[1] X. Li, T. Wan, J. Qiu, H. Wei, F. Qin, Y. Wang, Y. Liao, Z. Huang, and X. Tan, In-situ photocalorimetry-fluorescence spectroscopy studies of RhB photocatalysis over Z-scheme g-C_3N_4@Ag@Ag_3PO_4 nanocomposites: A pseudo-zero-order rather than a first-order process, *Appl. Catal. B* 217 (2017) 591–602. https://doi.org/10.1016/j.apcatb.2017.05.086.

[2] Y. Han, H. Yang, and X. Guo, Synthesis Methods and Crystallization of MOFs, in: Synthesis Methods and Crystallization, *IntechOpen*, 2020. https://doi.org/10.5772/intechopen.90435.

[3] C. Zhao, X. Pan, Z. Wang, and C.C. Wang, A critical review of MOF/bismuth-based semiconductor composites for boosted photocatalysis, *Chemical Engineering Journal* 417 (2021). https://doi.org/10.1016/j.cej.2020.128022.

[4] X. Yang, and D. Wang, Photocatalysis: From Fundamental Principles to Materials and Applications, *ACS Appl. Energy Mater*. 1 (2018) 6657–6693. https://doi.org/10.1021/acsaem.8b01345.

[5] M.A. Nasalevich, M. Van Der Veen, F. Kapteijn, and J. Gascon, Metal-organic frameworks as heterogeneous photocatalysts: Advantages and challenges, *CrystEngComm* 16 (2014) 4919–4926. https://doi.org/10.1039/c4ce00032c.

[6] C.B. Ong, L.Y. Ng, and A.W. Mohammad, A review of ZnO nanoparticles as solar photocatalysts: Synthesis, mechanisms and applications, *Renewable and Sustainable Energy Reviews* 81 (2018) 536–551. https://doi.org/https://doi.org/10.1016/j.rser.2017.08.020.

[7] S. Chandrappa, S.J. Galbao, A. Furube, and D.H.K. Murthy, Extending the Optical Absorption Limit of Graphitic Carbon Nitride Photocatalysts: A Review, *ACS Appl. Nano Mater*. 6 (2023) 19551–19572. https://doi.org/10.1021/acsanm.3c04740.

[8] H.A. Le Pham, D.T. Nguyen, V.C. Nguyen, and T. Ky Vo, Integrating Bi-containing metal–organic frameworks for enhancing their LED visible-light-driven photocatalytic activities towards Rhodamine dye, *Inorg. Chem. Commun*. 159 (2024) 111822. https://doi.org/10.1016/j.inoche.2023.111822.
[9] V.H. Nguyen, A.L.H. Pham, V.H. Nguyen, T. Lee, and T.D. Nguyen, Facile synthesis of bismuth(III) based metal-organic framework with difference ligands using microwave irradiation method, *Chemical Engineering Research and Design* 177 (2022) 321–330. https://doi.org/10.1016/j.cherd.2021.10.043.
[10] M.L. Zhang, C. Feng, W.X. Zhang, X.W. Luan, J. Jiang, and L.F. Li, Synthesis of bismuth nanoparticles by a simple one-step solvothermal reduction route, *in: Applied Mechanics and Materials*, 2013: pp. 155–158. https://doi.org/10.4028/www.scientific.net/AMM.423-426.155.
[11] M. Mahiuddin, and B. Ochiai, Green synthesis of crystalline bismuth nanoparticles using lemon juice, *RSC Adv*. 11 (2021) 26683–26686. https://doi.org/10.1039/d1ra03560f.
[12] V. Singh, D.K. Singh, M. Yadav, S. Singh, V. Rathour, A. Tiwari, and V. Ganesan, A Co and Fe bimetallic MOF with enhanced electrocatalytic oxygen evolution performance: exploring the electronic environment modifications upon Fe incorporation, *Energy Advances* 3 (2024) 636–647. https://doi.org/10.1039/D3YA00572K.
[13] V.C. Nguyen, T.D. Nguyen, Q. Thanh Hoai Ta, and A.L.H. Pham, Hierarchical structures of GO-supported BiBTC MOFs for efficient RhB photodegradation, *RSC Adv*. 15 (2025) 2779–2791. https://doi.org/10.1039/D4RA08337G.

VẬT LIỆU MOFs LƯỠNG KIM FeBiBTC LÀM XÚC TÁC QUANG HIỆU QUẢ CHO QUÁ TRÌNH PHÂN HỦY RHODAMINE B

NGUYỄN VĂN CƯỜNG, TRỊNH BẢO SƠN, PHẠM HOÀNG ÁI LỆ*

Khoa Công nghệ Hóa học, Trường Đại học Công nghiệp TPHCM

** Tác giả liên hệ: phamhoangaile@iuh.edu.vn*

Tóm tắt. Trong nghiên cứu này, vật liệu FeBiBTC-MOF được tổng hợp bằng phương pháp nhiệt dung môi và sử dụng làm xúc tác cho quá trình quang phân hủy Rhodamine B (RhB) trong dung dịch nước. Cấu trúc của vật liệu được đặc trưng bằng các kỹ thuật XRD, FT-IR và SEM. Kết quả cho thấy vùng cấm của FeBi-MOF (3,28 eV) thấp hơn so với BiBTC ban đầu (3,68 eV), góp phần cải thiện khả năng hấp thụ ánh sáng. Trong số các mẫu tổng hợp, FeBiBTC1 thể hiện hoạt tính quang xúc tác tốt nhất với hiệu suất phân hủy RhB đạt 99,58% sau 120 phút trong sự hiện diện của H_2O_2. Quá trình phân hủy tuân theo động học biểu kiến bậc nhất với hằng số tốc độ 0,045 phút^{-1}, cao hơn đáng kể so với vật liệu nền. Ảnh hưởng của các yếu tố đến phản ứng xúc tác quang phân hủy RhB như khối lượng xúc tác, pH, nồng độ chất màu và chất bắt gốc đã được khảo sát. Kết quả cho thấy các electron quang sinh đóng vai trò chủ đạo trong cơ chế phản ứng. Đồng thời, vật liệu cũng thể hiện khả năng tái sử dụng tốt, hoạt tính xúc tác giảm không đáng kể và duy trì độ ổn định cấu trúc sau bốn chu kỳ.

Từ khóa. Khung hữu cơ kim loại Bi, FeBiBTC, Rhodamine B, xử lý nước thải, oxy hóa nâng cao.

Received on April 20, 2026
Revised on June 01, 2026